Measuring charged current neutrino interactions in the Electromagnetic Calorimeters in near detector of T2K

Dominic Brailsford
TODO

A thesis submitted to Imperial College London
for the degree of Doctor of Philosophy

Abstract

To write

Declaration

This dissertation is the result of my own work, except where explicit reference is made to the work of others, and has not been submitted for another qualification to this or any other university. This dissertation does not exceed the word limit for the respective Degree Committee.

Dominic Brailsford

Acknowledgements

Something about my supervisor ...

Preface

This thesis describes my analysis of the ν_μ charged-current cross-section on lead using the T2K near detector electromagnetic calorimeters.

Contents

"These chickens jackin' my style. "

— Fergie

Chapter 1

Introduction

The field of neutrino physics is currently evolving very rapidly. With its tenuous postulation [1] acting as a future omen, the neutrino's mark on history would not become apparent from its discovery [2–4], but rather from a spate of surprising discoveries at the end of the 20th century [5–7] which conclusively proved that the Standard Model, while very successful, was incomplete. This revelation was experimental proof of Maki, Nagakawa and Sakata's extension [8] to Pontecorvo's theory of neutrino oscillation [9] with the inclusion of the Mikheyev-Smirnov-Wolfenstein (MSW) effect [10, 11]. The findings were groundbreaking as the underlying theory requires massive neutrinos, which is in direct contradiction to the Standard Model. The, now, standard theory of neutrino oscillation defines three neutrino flavours and three neutrino masses. However, the map between flavour and mass is not one-to-one, but rather a rotation of mass space onto flavour space. The main consequence of this rotation is that the flavour eigenstates are a superposition of mass eigenstates, namely

$$|\nu_\alpha\rangle = \sum_{i=k}^{3} U^*_{\alpha k} |\nu_k\rangle, \tag{1.1}$$

where $\alpha \in \{e, \mu, \tau\}$, ν_k are the neutrino mass eigenstates and $U^*_{\alpha k}$ is an element of a unitary rotation matrix which is known as the PMNS mixing matrix. As there are 3 mass and flavour eigenstates, the PMNS matrix is a 3×3 matrix and is often

parameterised as

$$U \equiv \begin{pmatrix} 1 & 0 & 0 \\ 0 & c_{23} & s_{23} \\ 3 & -s_{23} & c_{23} \end{pmatrix} \begin{pmatrix} c_{13} & 0 & s_{13}e^{-i\delta} \\ 0 & 1 & 0 \\ -s_{13}e^{i\delta} & 0 & c_{13} \end{pmatrix} \begin{pmatrix} c_{12} & s_{12} & 0 \\ -s_{12} & c_{12} & 0 \\ 0 & 0 & 1 \end{pmatrix}, \tag{1.2}$$

where $c_{ij} \equiv \cos\theta_{ij}$ and $s_{ij} \equiv \sin\theta_{ij}$. θ_{ij} are known as the mixing angles which parameterise how strong mixings between the flavour and mass eigenstates are and δ is a CP violating phase. The most surprising observable feature of this mechanism is the non-zero probability to detect a neutrino of specific flavour which was created at source in a different flavour state. By propagating the mass eigenstates through time, one can arrive at this probability which has the following form

$$P(\nu_\alpha \to \nu_\beta) = |\langle \nu_\beta | \nu\,(t) \rangle|^2 = |U_{\beta k} e^{-iE_k t} U^*_{\alpha k}|^2, \tag{1.3}$$

where $\nu\,(t)$ is the time-dependent neutrino mass eigenstate and E_k is the energy of the ν_k. For an accelerator-based neutrino oscillation experiment, the beam will be ν_μ dominated. So, the ν_μ survival probability, $P(\nu_\mu \to \nu_\mu)$, and ν_e appearance probability, $P(\nu_\mu \to \nu_e)$, which are typically of interest, can be approximated in the following forms

$$P(\nu_\mu \to \nu_\mu) \approx 1 - \cos^4\theta_{13} \sin^2 2\theta_{23} \sin^2\left(1.27 \frac{\Delta m^2_{23}}{(\mathrm{eV}^2)} \frac{L}{(\mathrm{km})} \frac{(\mathrm{GeV})}{E}\right) \tag{1.4}$$

$$P(\nu_\mu \to \nu_\mu) \approx \sin^2 2\theta_{13} \sin^2\theta_{23} \sin^2\left(1.27 \frac{\Delta m^2_{23}}{(\mathrm{eV}^2)} \frac{L}{(\mathrm{km})} \frac{(\mathrm{GeV})}{E}\right), \tag{1.5}$$

where $\Delta m^2_{ij} \equiv m^2_i - m^2_j$, L is the distance the neutrino propagates and E is the energy of the neutrino.

1.1 The state of the field

Data provided from a wide range of experiments show excellent agreement with the theory of neutrino oscillation and with a 3 flavour neutrino picture. Global fits applied to the data provided by these experiments gives best fit values for the oscillation

Parameter	best-fit ($\pm 1\sigma$)
Δm^2_{12} [10^{-5}eV^2]	$7.54^{+0.26}_{-0.22}$
$\lvert\Delta m^2\rvert$ [10^{-3}eV^2]	2.43 ± 0.06 (2.36 ± 0.06)
$\sin^2\theta_{12}$	0.308 ± 0.017
$\sin^2\theta_{23}$, $\Delta m^2 > 0$	$0.437^{+0.033}_{-0.023}$
$\sin^2\theta_{23}$, $\Delta m^2 < 0$	$0.455^{+0.039}_{-0.031}$
$\sin^2\theta_{13}$, $\Delta m^2 > 0$	$0.0234^{+0.0020}_{-0.0019}$
$\sin^2\theta_{13}$, $\Delta m^2 < 0$	$0.0240^{+0.019}_{-0.022}$
$\sin^2\theta_{13}$, $\Delta m^2 < 0$	$0.0240^{+0.019}_{-0.022}$
δ/π (2σ range quoted)	$1.39^{+0.38}_{-0.27}$ $(1.31^{+0.29}_{-0.33})$

Table 1.1: The best-fit values of the 3-neutrino oscillation parameters. $\Delta m^2 \equiv m^2_3 - \left(m^2_2 - m^2_1\right)/2$. The values (values in brackets) correspond to $m_1 < m_2 < m_3$ ($m_3 < m_1 < m_2$) [12].

parameters, which are summarised in table 1.1 [12]. The experiments which provided the data inputs to the global fit generally fall into one of four categories, with each category sensitive to a different subset of the neutrino oscillation parameters.

Solar neutrino experiments detect neutrinos generated in the core of the Sun as a result of nuclear reaction chains. Such experiments are primarily sensitive to θ_{12} and Δm^2_{12} which are often referred to as the solar mixing parameters. The final state neutrinos created in the Sun's core are MeV-scale ν_e but, because of propagation through the core's surrounding matter, the MSW effect results in a highly pure state of ν_2 at the Sun's surface. As ν_2 is a mass eigenstate, no oscillation occurs between the surface of the Sun and the Earth. Homestake [13], SAGE [14] and SNO [6] are examples of such experiments.

Reactor neutrino experiments measure $\bar{\nu}_e$ disappearance provided by inverse β decay in nuclear reactors with an average neutrino energy of 3 MeV. The baseline for oscillations varies between experiments, but a baseline of around 1 km provides excellent sensitivity to θ_{13}. Examples of reactor experiments are CHOOZ [15], Double CHOOZ [16], Daya Bay [17] and RENO [18].

Atmospheric neutrino experiments detect neutrinos which are produced when π and K mesons, created by cosmic rays interactions with the upper atmosphere of the

Earth, decay. The neutrinos produced are a mixture of ν_μ, $\bar{\nu}_\mu$, ν_e and $\bar{\nu}_e$. Because the cosmic ray flux is fairly uniform, atmospheric neutrino experiments are exposed to neutrinos from all directions, which results in a very wide range of oscillation baselines. The oscillation parameters that such experiments are sensitive to are θ_{23} and Δm^2_{13}. Super-Kamiokande [5] is an example of an atmospheric neutrino experiment.

Accelerator neutrino experiments produce beams of high purity ν_μ (or $\bar{\nu}_\mu$) at GeV-scale energy with wide ranging baselines which are generally $\mathcal{O}\,(100\text{ km})$. The highly man-made nature of such experiments allows almost complete control over L/E allowing careful tuning of parameter sensitivity. Accelerator neutrino experiments are generally sensitive to θ_{13}, θ_{23}, Δm^2_{13} and δ. K2K [19], MINOS [20], T2K [21] and NOνA [22]are examples of such experiments.

1.2 The future

It should be clear that an immense amount of progress has been made in the field, with remarkable contributions to the picture coming only in the last 20 years. However, there are several key questions which remain unanswered.

By far the most sought after answer is whether CP violation occurs in the lepton sector. The magnitude of CP violation is encapsulated in the CP violating phase δ and so it is this parameter which current and future long-baseline experiments are aiming towards. Currently, T2K and NOνA can provide the strongest constraints on δ. The future long-baseline experiments, Hyper-Kamiokande [23] and DUNE (formerly LBNE) [24] are being designed with a possible measurement of δ as a primary goal.

The second question still to be answered is the ordering of the mass eigenstates. Specifically is $m_3 \gg m_2 > m_1$ (the normal mass hierarchy) or $m_2 > m_1 \gg m_3$ (the inverted mass hierarchy)? The matter effects introduced by the MSW effect are mass hierarchy dependent. So, for very long-baseline experiments, there is mass hierarchy sensitivity. Currently NOνA is set to resolve the mass hierarchy problem. However, both Hyper-Kamiokande (via atmospheric measurements) and DUNE have measurement of the mass hierarchy as a primary goal.

Oscillation experiments only have the capability to measure the square of the mass

splitting differences. This means that all oscillation experiments have no sensitivity to the absolute neutrino mass scale and an entirely different type of neutrino experiment is required. Neutrinos are one of the final states associated with β decay and the mass of the neutrino should appear as a cut off in the β spectrum. The visibility of the cut-off entirely depends on the mass scale. So, the KATRIN experiment [25] will attempt to utilise the β decay feature, with a neutrino mass sensitivity of 0.2 eV.

It is not currently known whether neutrinos are their own anti-particle, otherwise known as Majorana neutrinos. A number of experiments are currently investigating this, all by searching for neutrinoless double β decay. A large neutrinoless double β decay experiment effort is ongoing, including EXO [26], SuperNEMO [27] and SNO+ [28].

While the long-baseline neutrino oscillation programme has been very successful, the short-baseline programme has seen several anomalies [29]. The LSND experiment found evidence of $\bar{\nu}_e$ in a $\bar{\nu}_\mu$ beam, which was consistent with neutrino oscillations [30]. However the data suggested a mass-squared splitting of 0.2-10 eV^2. This large splitting is consistent with a fourth species of neutrino. Because the data suggesting 3 flavours of weakly-interacting neutrino is strong, this postulated fourth species must be sterile. More recently, the MiniBooNE experiment observed a similar short baseline excess of $\bar{\nu}_e$ in a $\bar{\nu}_\mu$ beam with a mass-squared splitting of 0.01-1.0 eV^2 [31], further suggesting the sterile hypothesis. New experiments are now under development which aim to test this hypothesis, which include MicroBooNE [32] and SBND (formally LAr1-ND) [33].

Chapter 2

Neutrino interactions with atomic nuclei

The neutrino is a strictly weakly interacting particle. This has difficult implications for any experiment aiming to study neutrinos as particle detectors generally rely on the electromagnetic force. In fact, the only proven method of neutrino detection is to utilise a high mass target in which the neutrinos can interact with. Generally speaking, charged particles are produced by this interaction which can be detected by the usual means. The collected information from these charged final states can then be used to infer information about the incident neutrino. All neutrino experiments rely on this method and so any attempted measurements (e.g. δ) rely on our understanding on neutrino interactions with atomic nuclei. Our understanding of such processes is encompassed in the models we use to simulate the interactions.

2.1 Neutrino interactions at the GeV-scale

As the neutrino is weakly interacting, there are two channels available to a neutrino interacting with a nucleon: the Charge Current (CC) interaction in which a W boson is exchanged and the Neutral Current (NC) interaction in which a Z boson is exchanged. For neutrino energies below $\sim$1 GeV, the neutrino-hadron interactions are largely Quasi-Elastic (QE) [34]. In such an interaction, the incident neutrino scatters of the nucleon as if it were a single particle, rather than with one of the nucleon's constituent partons. In the case of a CCQE interaction, the neutrino is converted into its charged lepton equivalent and the target neutron converted to a proton. In the specific case of

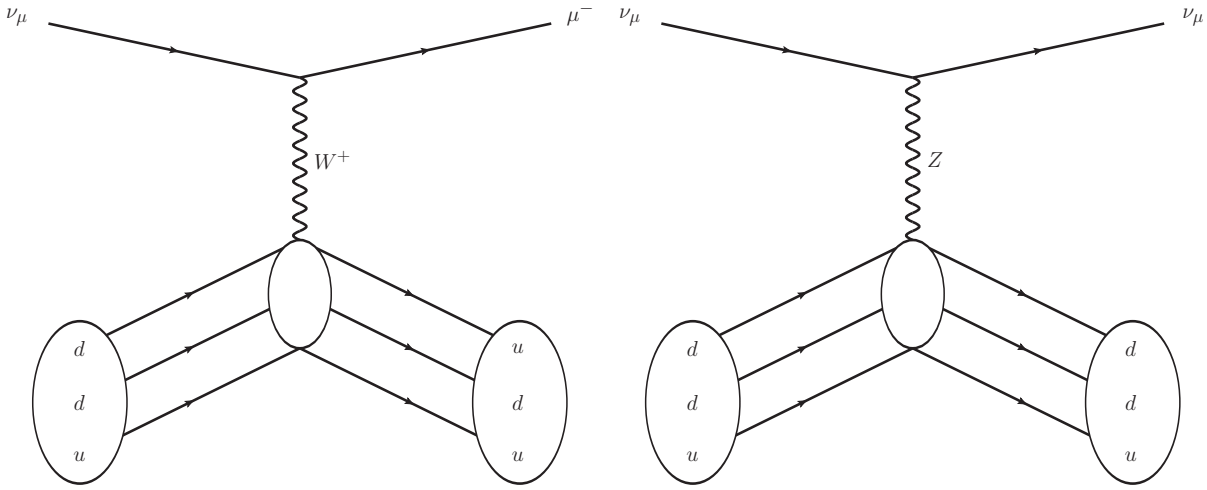

(a) CCQE. **(b)** NCQE.

Figure 2.1: Quasi-Elastic (QE) interactions of a ν_μ with a nucleon. The small ellipse represents the neutrino interacting with the nucleon as a whole, rather than with an individual parton.

an incident ν_μ, the interaction takes the following form

$$\nu_\mu n \rightarrow \mu^- p. \tag{2.1}$$

For NCQE interactions, the incident neutrino remains after the interaction has occurred and no nucleon conversion takes place. Because of this fact, the target nucleon in a NCQE interaction need not be a neutron. So, for ν_μ NCQE interactions, there are two channels available

$$\nu_\mu n \rightarrow \nu_\mu n, \tag{2.2}$$

$$\nu_\mu p \rightarrow \nu_\mu p. \tag{2.3}$$

The two kinds of QE interaction are shown in Fig. 2.1.

For higher energy neutrinos, there is sufficient energy to promote the target nucleon to an excited state. A quick after-effect of this promotion is that the excited state decays, resulting in further particle emission. This interaction topology, which dominates in the 1 GeV to 5 GeV energy range, is known as RESonant pion (RES) production as the neutrino interaction produces Δ resonance which typically decays to a nucleon and a

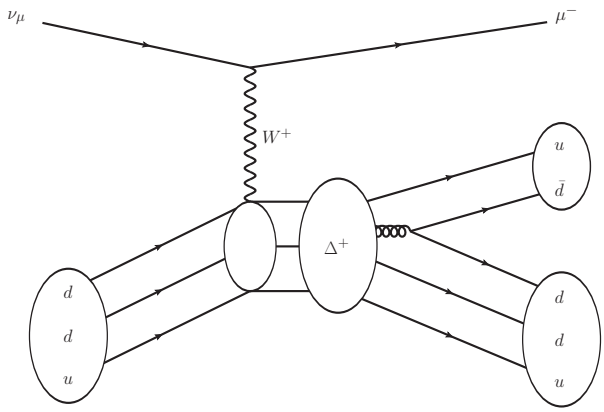

Figure 2.2: A Charged Current RESonant pion (CCRES) interaction of a ν_μ with a neutron. The Δ resonance decays to a neutron and a π^+.

single pion in the final state. In the case of ν_μ CCRES, the interaction generally takes the following form

$$\nu_\mu N \rightarrow \mu^- N^*, \tag{2.4}$$

$$N^* \rightarrow \pi N', \tag{2.5}$$

where $N, N' = n, p$. An example diagram of a ν_μ-CCRES interaction with a π^+ in the final state is shown in Fig. 2.2.

For neutrinos with energy above the RES-dominant region, the neutrino has enough energy to penetrate the nucleon and scatter off an individual quark. Because of the nature of the strong force, the scattered quark and the nucleon remnant produce a hadronic shower in the final state. This process is known as Deep Inelastic Scattering (DIS). For ν_μ-CCDIS, the interaction takes the following form

$$\nu_\mu N \rightarrow \mu^- X, \tag{2.6}$$

where X is the remnant of the nucleus after the interaction occurs. An example diagram of a ν_μ-CCDIS interaction is shown in Fig. 2.3.

While the value of a particular interaction cross-section should depend on the nuclear environment, it is possible to make comparisons of the measured cross-section per nucleon. Fig. 2.4 shows a comparison of ν_μ CC cross-section measurements per nucleon

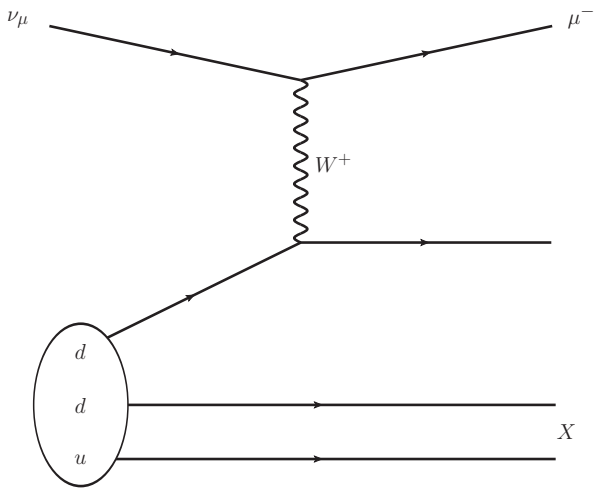

Figure 2.3: A Charged Current Deep Inelastic Scattering (CCDIS) interaction of a ν_μ with a neutron. X resembles the leftover nuclear remnant.

from different experiments, all of which sample a different neutrino energy range. There are large uncertainties for many of the cross-section measurements, particularly for the ones sampling the lower energy ranges. The T2K beam energy is $\sim$700 MeV, which sits in the region of higher uncertainty.

CCQE interactions are experimentally the most interesting and this is the interaction region where most recent measurements have been focused. Because of the simplicity of the CCQE topology, the interaction can be treated as a two-body scatter. So, by applying simple conservation rules, the neutrino energy can be kinematically reconstructed. In such interactions, the nucleon structure is parameterised using a set

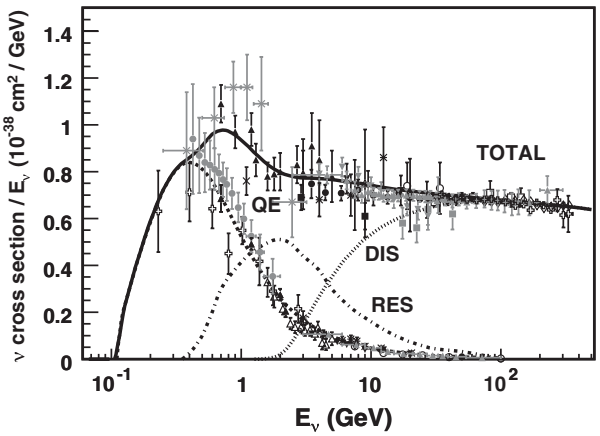

Figure 2.4: ν_μ CC cross-section measurements per nucleon for a range of energies, showing the QE, RES and DIS contributions [34].

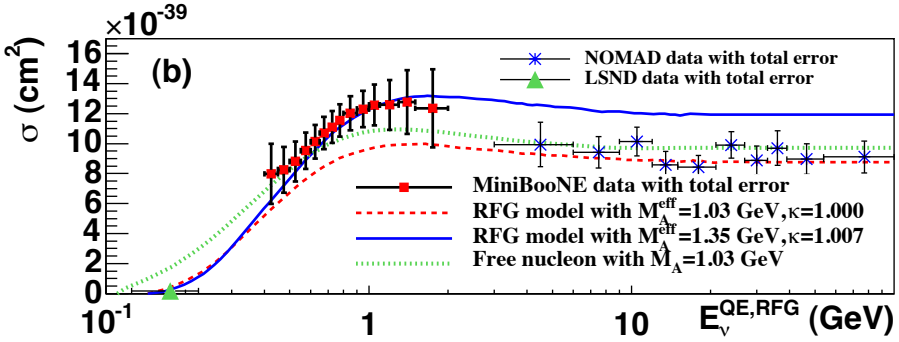

Figure 2.5: The CCQE cross-sections measured by the MiniBooNE and NOMAD experiments. The solid and dashed lines represent models with different values of M_A [36].

of form factors, the most interesting of which is the axial-vector form factor, $F_A(Q^2)$. $F_A(Q^2)$ has been, and still is, assumed to take a dipole form

$$F_A(Q^2) = \frac{F_A(0)}{(1 - Q^2/M_A^2)^2}, \tag{2.7}$$

where Q^2 is the negative of the squared four-momentum transfer of the lepton to the hadron, $F_A(0) = 1.2694 \pm 0.0028$ [35], and M_A is known as the axial mass. Recent measurements of the CCQE cross-section by the MiniBooNE [36] and NOMAD [37] experiments have sparked interest by reporting measured cross-sections which are in tension with one another, the results of which shown in Fig. 2.5. A popular explanation for this discrepancy is a lack of understanding of the nuclear environment. Because the neutrino is not scattering of a free nucleon, but rather a nucleon in a strongly contained system, experiments actually measure an effective M_A. It is possible that the nuclear effects cause a modification to the effective M_A that the experiments measure. This possible explanation for the discrepancy has placed a heavier emphasis on nuclear modelling in neutrino interaction experiments.

2.2 Neutrino interactions with heavy nuclei

As introduced above, consideration of nuclear effects in cross-section measurements is important. This is especially true for neutrino interactions on heavy target nuclei. As one can imagine, the presence of a nucleus can dramatically effect the interactions that are observed in a detector. A popular model for the nucleus is the Relativistic Fermi-Gas (RFG) model [38]. The RFG model treats the nucleus as a collection of

non-interacting nucleons sitting in a potential well. The nucleons are stacked in the potential well according to the Pauli exclusion principle. This leads to a uniform momentum distribution of the nucleons up to the Fermi momentum p_F. Importantly, the Pauli exclusion principle has a further effect. Because the final state nucleon is forbidden from occupying a state taken by another nucleon in the potential well, the energy transfer of the neutrino to the nucleon must result in a final state nucleon with a momentum above p_F, resulting in a reduction of the cross-section.

The RFG can only model the effect of the nucleus on the initial neutrino interaction which creates the final states. However, these final states are created within the nucleus and so additional interactions of the final states with the nucleus can occur. The Final-State Interactions (FSI) can significantly alter the momentum and direction of the final-state particles. As the final-state particles are used to infer neutrino properties, the FSI effects can alter the interpretation of the reconstructed events. In simulation, variations of the cascade model are typically used. This involves pushing the final-state particles through the nucleus in discreet steps and, at each step, probabilistically updating the particle properties. If at any point a final-state particles knocks out another nucleon, the additional nucleon is also pushed through the nucleus in parallel. The discreet stepping occurs until all relevant particles have escaped the nucleus.

To test such cross-section models, including nuclear effects, it is necessary to compare prediction with collected data. However, collected cross-section data for heavy nuclei is relatively sparse. In the case of lead, only two experiments have performed cross-section measurements. The first measurement was performed by the CHORUS [39] experiment. The CHORUS detector, exposed to the CERN SPS beam with a wide-band ν_μ beam of 27 GeV average energy, measured a cross-section for lead, iron, marble and polyethylene. However, because the absolute flux was not measured in the experiment, all of the cross-section measurements were normalised to a common constant. Their results are summarised in Fig. 2.6. The second measurement was made by the MINERνA experiment [40], which used the Fermilab NuMI beam with a 8 GeV average energy, to measure the relative ν_μ CC cross-section on lead to that of plastic scintillator as a function of neutrino energy. Their results, shown in Fig. 2.7, largely agreed with the prediction.

As neutrino oscillation physics enters the precision era, it is becoming increasingly important that our understanding of neutrino cross-sections is improved. To achieve this

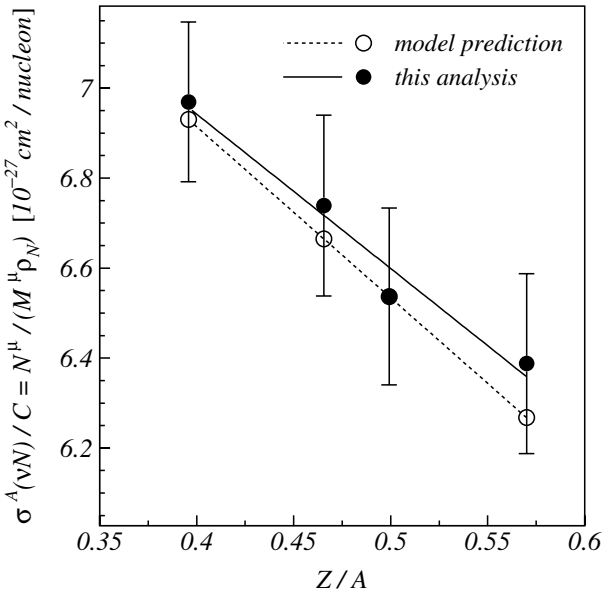

Figure 2.6: Measured values of the ν_μ CC relative cross-section for several elements. The black and white points are the collected data and prediction respectively. The solid and dashed lines are the linear best fit lines to the data and prediction respectively. Going from left to right, the points represent data/prediction for lead, iron marble and polyethylene.

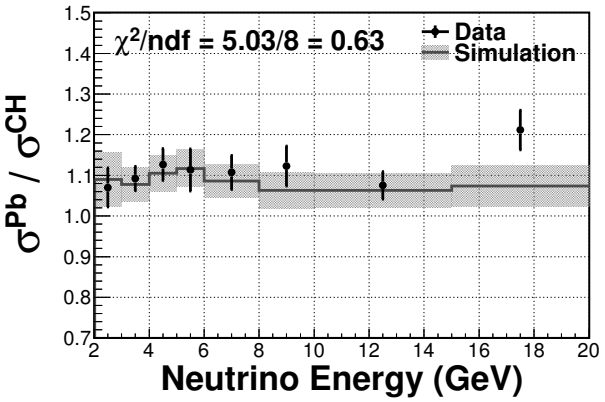

Figure 2.7: Ratio of the measured ν_μ CC inclusive cross-section on lead to plastic scintillator as a function of neutrino energy. The error bars on the simulation (data) are statistical (systematic) uncertainties [40].

goal, more cross-section measurements across a range of nuclear targets are needed. This thesis presents a measurement of the ν_μ CC inclusive cross-section on lead using the electromagnetic calorimeters contained in the near detector of the T2K experiment.

Bibliography

[1] W. Pauli, Open letter to the Gauverein meeting in Tubingen, 1930.

[2] C. L. Cowan, F. Reines, F. B. Harrison, H. W. Kruse, and A. D. McGuire, Science **124**, 103 (1956).

[3] G. Danby *et al.*, Phys. Rev. Lett. **9**, 36 (1962).

[4] K. Kodama *et al.*, Physics Letters B **504**, 218 (2001).

[5] Y. Fukuda *et al.*, Phys. Rev. Lett. **81**, 1562 (1998).

[6] Q. R. Ahmad *et al.*, Phys. Rev. Lett. **87**, 071301 (2001).

[7] K. Eguchi *et al.*, Phys. Rev. Lett. **90**, 021802 (2003).

[8] Z. Maki, M. Nakagawa, and S. Sakata, Progress of Theoretical Physics **28**, 870 (1962).

[9] B. Pontecorvo, JETP Lett. **33**, 549 (1957).

[10] L. Wolfenstein, Phys. Rev. D **17**, 2369 (1978).

[11] S. Mikheev and A. Y. Smirnov, Sov.J.Nucl.Phys. **42**, 913 (1985).

[12] Particle Data Group, K. Olive *et al.*, Chin.Phys. **C38**, 090001 (2014).

[13] B. T. Cleveland *et al.*, The Astrophysical Journal **496**, 505 (1998).

[14] J. N. Abdurashitov *et al.*, Phys. Rev. C **80**, 015807 (2009).

[15] M. Apollonio *et al.*, The European Physical Journal C - Particles and Fields **27**, 331 (2003).

[16] Y. Abe *et al.*, Physics Letters B **723**, 66 (2013).

[17] F. P. An *et al.*, Phys. Rev. Lett. **108**, 171803 (2012).

[18] J. K. Ahn *et al.*, Phys. Rev. Lett. **108**, 191802 (2012).

[19] M. H. Ahn *et al.*, Phys. Rev. D **74**, 072003 (2006).

[20] D. G. Michael *et al.*, Phys. Rev. Lett. **97**, 191801 (2006).

[21] (T2K Collaboration), K. Abe *et al.*, Phys. Rev. Lett. **112**, 061802 (2014).

[22] NOvA, D. Ayres *et al.*, (2004), hep-ex/0503053.

[23] Hyper-Kamiokande Working Group, K. Abe *et al.*, (2014), 1412.4673.

[24] LBNE, C. Adams *et al.*, (2013), 1307.7335.

[25] C. Weinheimer, Progress in Particle and Nuclear Physics **48**, 141 (2002).

[26] M. Auger *et al.*, Phys. Rev. Lett. **109**, 032505 (2012).

[27] A. Barabash and the SuperNemo Collaboration, Journal of Physics: Conference Series **375**, 042012 (2012).

[28] SNO+, M. C. Chen, (2008), 0810.3694.

[29] J. Fan and P. Langacker, Journal of High Energy Physics **2012** (2012).

[30] LSND, A. Aguilar-Arevalo *et al.*, Phys.Rev. **D64**, 112007 (2001), hep-ex/0104049.

[31] MiniBooNE, A. Aguilar-Arevalo *et al.*, Phys.Rev.Lett. **110**, 161801 (2013), 1207.4809.

[32] C. M. Ignarra, ArXiv e-prints (2011), 1110.1604.

[33] LArTPC, C. Adams *et al.*, (2013), 1309.7987.

[34] J. A. Formaggio and G. P. Zeller, Rev. Mod. Phys. **84**, 1307 (2012).

[35] K. Nakamura and P. D. Group, Journal of Physics G: Nuclear and Particle Physics **37**, 075021 (2010).

[36] A. A. Aguilar-Arevalo *et al.*, Phys. Rev. D **81**, 092005 (2010).

[37] V. Lyubushkin *et al.*, The European Physical Journal C **63**, 355 (2009).

[38] R. Smith and E. Moniz, Nucl.Phys. **B43**, 605 (1972).

[39] The European Physical Journal C - Particles and Fields **30**, 159 (2003).

[40] (MINERvA Collaboration), B. G. Tice *et al.*, Phys. Rev. Lett. **112**, 231801 (2014).

List of Figures

List of Tables